2013 European Control Conference (ECC)
July 17-19, 2013, Zürich, Switzerland.

Computing Optimal Operating Condition Profiles for Fed-Batch Fermentation of Fuel-Grade Ethanol

Wei Dai and Juergen Hahn

Abstract—**This paper investigates optimization of operational strategies of an industrial ethanol fermentation process. One of the challenges associated with this type of process is that most of the measurements are only taken sporadically, thereby, complicating process monitoring and optimization. The one exception to this rule involves temperature measurements, which are readily available. However, existing models used in industry do not include an energy balance and, accordingly, the temperature measurements cannot be used to estimate model parameters. This paper addresses these deficiencies and proposes modifications to an existing ethanol fermentation model. The proposed changes include the derivation of an energy balance, modification of the reaction kinetics to include additional inhibition terms, and also estimation of model parameters from industrial data. The new model is validated against plant data and then used for optimization of the process operations. It is shown that modifications of the input profiles for the cooling rate and the glucoamylase addition can lead to an approximately 10% increase in ethanol yield. These are promising results, even though these findings will ultimately need to be validated during real plant operations.**

I. Introduction

Ethanol produced from fermentation of biomass-derived sugar is increasingly being used as a transportation fuel, either neat or in petrol blends. The U.S. is the world's largest biofuel producer with an expected production of 57 billion liters of ethanol in 2012 which is estimated to rise to 136 billion liters by 2022 [1]. Most of the ethanol in the U.S. is produced in maize-based plants, and more than 90% of the plants make use of the dry mill process. During this process, the simultaneous saccharification and fermentation (SSF) is the most important step, where dextrin is broken down into fermentable dextrose by glucoamylase and dextrose is converted into ethanol by yeast. The theoretical maximum yield of ethanol produced from maize starch correlates to an ethanol concentration after SSF of over 160 (g/L) [2]. Currently, the most advanced commercial plants can produce approximately 150 (g/L), however, the average yield from plants using traditional techniques is less than 140 (g/L). Therefore, improving the operations of SSF based on current facilities is undoubtedly the most economic approach to increase ethanol yield. However, optimization of SSF operations requires a good understanding of the process, in the form of data and/or models.

One significant challenge for the use of SSF models in commercial plants is the lack of data, since yeast and other intermediate substances cannot be measured independently, and dextrose and ethanol concentrations can only be measured every few hours. The one process variable that is measured at a high frequency is the temperature, however, an energy balance is required if these temperature data are to be used for parameter estimation or monitoring other quantities. Unfortunately, none of the existing models for SSF include an energy-balance equation.

Another challenge for operating ethanol plants is that ethanol fermentation is an exothermic process and temperature changes will significantly affect enzyme and yeast activity. Glucoamylase has an optimum activity at 140ºF for saccharification, while the optimal temperature for yeast growth and fermentation is in the range of 84-94ºF. These competing optimal temperatures highlight the complexity of selecting an optimal temperature profile over the course of a batch. It should be noted that most commercial plants hold the temperature constant between 86-90ºF.

This work addresses the above mentioned challenges by: (i) establishing the relationship between cooling water flowrate, temperature, and active yeast concentration, so that temperature data can be used to estimate unknown parameters arising from component balances and the proposed energy balance; (ii) computing optimal input profiles for the fermenter by solving a dynamic optimization problem involving the developed model.

The paper is structured as follows: preliminaries about the process and an existing commercial model are presented in Section II. The model development is presented in Section III. The optimization problem for determining optimal input profiles is formulated and solved in Section IV. Conclusions are presented in Section V.

II. Preliminaries

A. Description of industrial ethanol fermentation

Fuel-grade corn ethanol is produced in one of two ways, using either the wet mill or the dry mill process. This work focuses on dry-mill-based plants, where the entire grain kernel is ground into flour, and the flour is transported into the cook tank, allowing for complete water penetration. Then, the starch inside the flour is hydrolyzed into dextrin as it passes through the liquification tank as shown in Fig. 1.

Manuscript received October 2, 2012. This work was supported in part by the U.S. National Science Foundation under Grant 0941313, Rockwell Automation, and the Process Science Technology Center.

J. Hahn is a professor in the Department of Biomedical Engineering and the Department of Chemical & Biological Engineering at the Rensselaer Polytechnic Institute, Troy, NY 12180 USA (phone: 518-276-2138; fax: 518-276-3035; e-mail: hahnj@rpi.edu).

W. Dai is in the Department of Chemical & Biological Engineering at the Rensselaer Polytechnic Institute, Troy, NY 12180 USA.

Dextrin, the mixture of different long-chain sugars (maltose, D_3, D_4 to D_7), then enters the batch fermenter and undergoes a simultaneous saccharification and fermentation process in response to the addition of enzymes and yeast from the propagation tank. A general overview of the SSF process and a timeline describing batch operation is shown in Fig. 2.

LIST OF SYMBOLS

F_{Prop}	*l/hr*	flowrate from the propagation tank
F^0_{Prop}	*l/hr*	designed flowrate from the propagation tank
t_{start}	*hr*	time point that the enzyme starts to flow into the fermenter
t_{drop}	*hr*	time point that the enzyme stops flowing into the fermenter
F_{Slurry}	*l/hr*	flowrate from the liquification tank
F^0_{Slurry}	*l/hr*	designed flowrate from the liquification tank
V	*l*	liquid volume in the fermenter
V_{full}	*l*	volume of the fermenter
V_{GA}	*l*	volume of the glucoamylase in the fermenter
F_{GA}	*l/hr*	flowrate of glucoamylase
y_{GA}	*g/l*	concentration of glucoamylase in the fermenter
ρ_{GA}	*g/l*	density of glucoamylase
y_{Dex}	*g/l*	concentration of dextrin in the fermenter
y^{IN}_{Dex}	*g/l*	concentration of dextrin from liquification tank
y_{dex}	*g/l*	concentration of dextrose in the fermenter
y_{active}	*g/l*	concentration of active yeast in the fermenter
y_{lag}	*g/l*	concentration of lag yeast in the fermenter
y^0_{lag}	*g/l*	concentration of lag yeast from propagation tank
y_{EtOH}	*g/l*	concentration of ethanol in the fermenter
y^0_{EtOH}	*g/l*	concentration of ethanol from liquification tank
T	*°F*	temperature inside the fermenter
T_{ref}	*°F*	reference temperature used to calculate internal energy
H_{feed}	*Btu/hr*	internal energy from the slurry flow and yeast flow
H_{cool}	*Btu/hr*	heat taken away by cooling facility
F_{cool}	*gal/hr*	flowrate of cooling water
ρ	*g/l*	density of the liquid in the fermenter
C_p	*Btu/°F/l*	heat capacity of the liquid in the fermenter
r_{GA}	hr^{-1}	dextrin → dextrose conversion rate
μ_a	hr^{-1}	dextrose → ethanol conversion rate
μ^{max}_a	hr^{-1}	maximum dextrose → ethanol conversion rate
μ_{lag}	hr^{-1}	lag yeast → active yeast conversion rate
μ^{max}_{lag}	hr^{-1}	maximum lag yeast → active yeast conversion rate
μ_s	hr^{-1}	dextrose consumption rate
μ^{max}_s	hr^{-1}	maximum dextrose consumption rate
μ_x	hr^{-1}	active yeast growth rate
μ^{max}_x	hr^{-1}	maximum active yeast growth rate
r_d	hr^{-1}	active yeast death rate
f_a		ethanol inhibition factor

B. Commonly used SSF model

The starting point of the modeling effort of this paper is a model which has been extensively used for commercial fuel-grade ethanol production. The model originates from references [3-9], and the equations fall into three categories: (i) Equations (1) – (13) include the dynamic balances from [3-5, 7, 8]; (ii) Equations (14) – (18) contain the kinetic expressions from [3-6, 8, 9]; and (iii) Equations (19) – (23) include the temperature influence from [3, 8].

The differential equations in the model describe the mass and component balances (glucoamylase, dextrin, dextrose, lag yeast, active yeast, and ethanol) of the process inside the batch fermenter. The description of each variable can be found in the list of symbols. In addition, $H(\ldots)$ is the Heaviside function and $x_{1,\ldots,3}$ are introduced for notational purposes.

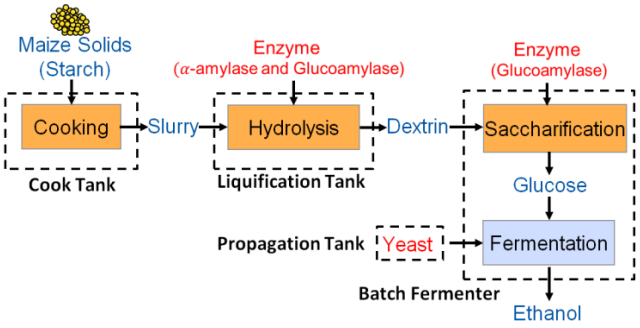

Fig. 1. Flow chart of the dry mill process.

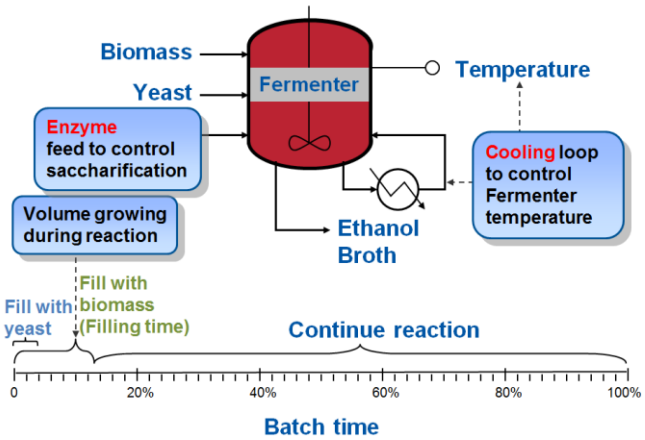

Fig. 2. Overview of SSF process and timeline of batch operation.

$$\frac{dV}{dt} = F_{Prop} + F_{Slurry} \tag{1}$$

$$\frac{dV_{GA}}{dt} = F_{GA} \tag{2}$$

$$\frac{dy_{GA}}{dt} = \frac{F_{GA}\rho_{GA}}{V} - x_3 y_{GA} \tag{3}$$

$$\frac{dy_{Dex}}{dt} = x_1 y^{IN}_{Dex} - x_3 y_{Dex} - r_{GA} y_{Dex} \tag{4}$$

$$\frac{dy_{dex}}{dt} = r_{GA} y_{Dex} - \mu_s y_{active} - x_3 y_{dex} \tag{5}$$

$$\frac{dy_{lag}}{dt} = \left(-\mu_{lag} - x_3\right) y_{lag} + x_2 y^0_{lag} \tag{6}$$

$$\frac{dy_{active}}{dt} = \left(\mu_x - r_d - x_3\right) y_{active} + \mu_{lag} y_{lag} \tag{7}$$

$$\frac{dy_{EtOH}}{dt} = \mu_a f_a y_{active} - x_3 y_{EtOH} + x_1 y^0_{EtOH} \tag{8}$$

$$F_{Prop} = F^0_{Prop} \cdot \left[1 - H\left(t - t_{drop}\right)\right] \cdot H\left(t - t_{start}\right) \tag{9}$$

$$F_{Slurry} = F^0_{Slurry} \cdot \left[1 - H\left(V - V_{full}\right)\right] \tag{10}$$

$$x_1 = \frac{F_{Slurry}}{V} \tag{11}$$

$$x_2 = \frac{F_{Prop}}{V} \tag{12}$$

$$x_3 = x_1 + x_2 = \frac{F_{Slurry} + F_{Prop}}{V} \tag{13}$$

Equations (1) - (13) describe the SSF process from the beginning of the filling phase to the end of batch fermentation. In order to avoid introducing more complexity to the model, dextrin is assumed to be directly broken down into dextrose without considering intermediate steps. This assumption is a trade-off between model accuracy and complexity as including additional steps would also result in additional parameters which would introduce more uncertainty. The kinetic expressions in the dynamic balances are given by:

$$r_{GA} = \frac{\mu_{GA}^{\max} y_{GA}}{k_{GA} + y_{Dex}} \tag{14}$$

$$\mu_s = \frac{\mu_s^{\max} y_{dex}}{k_s + y_{dex}} \tag{15}$$

$$\mu_a = \frac{\mu_a^{\max} y_{dex}}{k_s + y_{dex}} \tag{16}$$

$$\mu_x = \frac{\mu_x^{\max} y_{dex}}{(k_{x1} + y_{EtOH})(k_{x2} + y_{dex})} \tag{17}$$

$$f_a = 1 - \alpha y_{EtOH} \tag{18}$$

Equations (14) - (17) are modified Michaelis-Menten functions which use Monod kinetics. Equation (17) describes the effect of saturation and dependence of the reaction rate on the concentration of the substrates. Equation (18) represents an additional factor for describing active yeast product inhibition.

The effect of the temperature on several of the model parameters is captured by the following expressions:

$$\mu_{GA}^{\max} = d_1 \exp\left[\gamma_1 \left(a_1 T + b_1\right)\right] \tag{19}$$

$$\mu_s^{\max} = d_2 \exp\left[\gamma_2 \left(a_2 T + b_2\right)\right] \tag{20}$$

$$\mu_a^{\max} = d_3 \exp\left[\gamma_3 \left(a_3 T + b_3\right) + c_3\right] \tag{21}$$

$$\mu_x^{\max} = d_4 \gamma_4 \exp\left(a_4 T + b_4\right) \tag{22}$$

$$r_d = d_5 \exp\left(a_5 T + b_5\right) \tag{23}$$

Arrhenius-type equations are used to describe the temperature effect on the enzyme and yeast activity, where $a_{1,\ldots,5}$, $b_{1,\ldots,5}$, $c_{2,3}$, $d_{1,\ldots,5}$, are known parameters, and $\gamma_{1,\ldots,4}$, are unknown parameters that need to be estimated. Data for this model were collected at higher frequency than normal and the fermenter was operated at different, but constant, temperatures. The unknown parameters, which need to be estimated, were identified by local sensitivity analysis. It is important to note that this model describes the effect of temperature on the system, however, the effect of the exothermic reactions and cooling of the process is not captured in the model as the model contains no energy balance.

III. Model development

A. Simultaneous substrate and product inhibition

Simultaneous elevated concentrations of dextrose and ethanol during the SSF process exhibit synergistic stress on the yeast and can cause incomplete fermentation. The fermentation process needs to be carefully managed to minimize this type of stress. As dextrose is produced and consumed during the process, its concentration reaches its highest level at some point during the batch, whereas the amount of ethanol steadily increases as ethanol represents the final product of this process. Equation (17) uses a Monod kinetics expression to reflect the effect of saturation; however, this expression has been replaced in this work by a Haldane kinetics term to better represent the simultaneous substrate and product inhibition:

$$\mu_x = \frac{\mu_x^{\max} y_{dex}}{\left(k_{x1} + y_{EtOH}\right)\left(k_{x2} + y_{dex} + \frac{y_{dex}^2}{k_{x3}}\right)} \tag{24}$$

Furthermore, maintaining the dextrose concentration within a certain range forms the most important path constraint for dynamic optimization of this process which will be further discussed in Section IV. The use of Haldane kinetics can indirectly simplify the optimization problem as the inhibition term will more accurately reflect the lower reaction rates and thereby more easily keep the dextrose concentration within the path bound. However, it should be noted that this modification of the model was made to more accurately reflect the process and not for ease of computation.

B. Development of energy balance

While several papers describing SSF models can be found in the open literature, none of the models include an energy balance which reflects the relationship between temperature, the heat released by the ongoing reactions, and the cooling mechanism.

In this work, several assumptions are made for deriving the energy balance: (i) the density ρ and the heat capacity C_P are constant; (ii) the heat of reaction ($-\Delta H$) is constant, and only the heat generated by the fermentation (Equation (8)) is included; (iii) heat loss of the system to the surrounding area is neglected; Based upon these assumptions, the energy balance of the fermenter can be written as

$$\frac{d\left\{\rho V C_P \left(T - T_{ref}\right)\right\}}{dt} = \left(H_{feed} - H_{cool}\right) + H_{reaction} \tag{25}$$

$$H_{reaction} = \left(-\Delta H\right)\mu_a f_a y_{active} V \tag{26}$$

Here, T_{ref} denotes the reference temperature that is used to calculate the enthalpy of each substance; the initial temperature T_0 of the mash slurry from the liquification tank is usually used as T_{ref}; H_{feed} denotes the total enthalpy of the mash slurry from the liquification tank and the enthalpy of the yeast flow from the propagation tank; H_{cool} represents the heat removed by the cooling water and has a linear relationship

with F_{cool}; $H_{reaction}$ represents the enthalpy produced during the fermentation process.

Rearranging (25) and substituting results in

$$\frac{dT}{dt} = \frac{H_{feed} - H_{cool}}{\rho C_P V} + \frac{(-\Delta H)\mu_a f_a y_{active}}{\rho C_P} - x_3(T - T_{ref}) \quad (27)$$

While the energy balance shown in Equation (27) is straightforward, it includes several parameters whose values are not easy to determine as they are not constant. For example, as the reaction proceeds, solid particles inside the slurry dissolve into the solution and gas products escape from the solution, changing the concentration of each substance. Therefore, density and heat capacity vary with changes of the components in the fermenter, even though one of the assumptions made above was that these properties are constant. In addition to generating heat, energy from the consumption of dextrose is also used for the growth of active yeast and the production of other byproducts. This effect is also influenced by the concentrations of the components and other conditions in the fermenter. In order to capture all the uncertainties and correlate them with concentrations of components in the fermenter, the factors ψ_1 and ψ_2, shown in (28), have been introduced.

$$\frac{dT}{dt} = \psi_1 \frac{H_{feed} - H_{cool}}{\rho C_P V} + \psi_2 \frac{(-\Delta H)\mu_a f_a y_{active}}{\rho C_P} - x_3(T - T_{ref}) \quad (28)$$

$$\psi_1 = \Gamma_1 + \Gamma_2 y_{EtOH} \quad (29)$$

$$\psi_2 = \Gamma_3 + \Gamma_4 y_{EtOH} + \Gamma_5 y_{EtOH}^2 \quad (30)$$

While there is no specific reason why these factors are expressed in this form, it has been found that this type of expression provided significantly better results for the temperature than other expressions, such as higher or lower polynomials, polynomials which also depended upon other concentrations, etc., when applied to the available plant data sets.

C. Parameter estimation and model validation

The model includes nine unknown parameters which need to be estimated: $\gamma_{1,\ldots,4}$ deal with uncertainty in the kinetic expressions, while $\Gamma_{1,\ldots,5}$ capture the uncertainty in the energy balance. The data set used for training includes dextrose concentration, ethanol concentration, and temperature from Batch 001. Since there are significantly more data points for the temperature than for the concentration, the numerical weight placed on the data is adjusted so that each data set is weighted equally during parameter estimation.

Parameter values have been estimated using a Trust-Region approach for the optimization which repeatedly solves the model using a fixed-step 5th order Runge-Kutta integrator, and the values are summarized in Table I. It is worth noting that a fixed-step Runge-Kutta method is used for each integration step rather than a variable-step method since variable-step method will introduce additional "noise" to the optimization process that may greatly reduce the efficiency.

TABLE I
ESTIMATED VALUES OF UNKNOWN PARAMETERS

γ_1	γ_2	γ_3	γ_4	Γ_1	Γ_2	Γ_3	Γ_4	Γ_5
1.278	0.432	0.217	0.940	1.039	-0.005	647.675	-7.573	0.029

TABLE II
INITIAL CONDITIONS OF THE SSF MODEL

V^0	V_{GA}^0	y_{GA}^0	y_{lag}^0	y_{active}^0	$y_{dextrin}^0$	$y_{dextrose}^0$	$y_{ethanol}^0$	T^0
5000 gal	0 gal	0 g/L	0 g/L	0 g/L	244 g/L	10 g/L	4 g/L	92 °F

The system can be simulated using these parameter values and the initial conditions presented in Table II. Simulation results of several states of the system are shown in Fig. 3. It can be seen that the simulated dextrose concentration, ethanol concentration, and temperature match the experimental data with a good degree of accuracy for this process. Furthermore, simulations have been carried out for four other batches (Batch 002, Batch 003, Batch 004, and Batch 005), where simulation results also fit the experiment data very well.

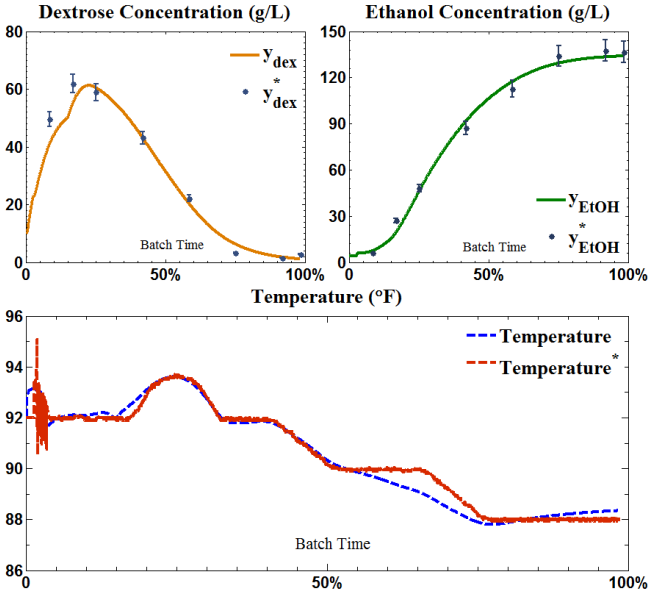

Fig. 3. Simulation result with estimated parameters (Batch 001).

IV. Determination of Optimal Input Profile

A. Optimization problem formulation

As the derived model has been validated in Section III, it is now possible to use this model for determining improved operating conditions for SSF. Since the state variables undergo significant changes during SSF, there is no steady state and thus no constant set points over the course of a batch. Therefore, the major objective is to manipulate the input variables (cooling water flowrate and the enzyme injection) to follow reference trajectories which maximize the ethanol concentration at the end of the run. This problem belongs to the category of dynamic optimization problems [10]. The mathematical formulation is shown below:

$$\max_{u} \; y = x_{EtOH}\left(t_f\right) \tag{31}$$

$$s.t. \;\; \dot{x} = F(x,\gamma,u), x(0) = x_0 \tag{32}$$

$$\mathrm{P}(x,u) \le 0, \Omega\left(x\left(t_f\right)\right) \le 0 \tag{33}$$

Equations (32) – (33) represent the dynamic system with known initial values x_0 , the path constraint P and the terminal constraint Ω . The model can be formulated as a nonlinear programming problem by discretizing the continuous differential equation model into an algebraic model using a three-point Radau collocation on finite elements [11, 12]. Then, the optimization problem is implemented in AMPL [13], and is solved using the nonlinear solver IPOPT [14].

B. Dynamic optimization result and analysis

Solution of the dynamic optimization problem returns the optimal profiles shown in Fig. 4. It can be seen that the optimal temperature profile remains high during the filling phase, but rapidly drops to the lower operating condition towards the end of the filling phase and remains there for most of the batch time. The temperature slightly rises towards the end of the batch as no cooling is taking place and the fermentation still produces a small amount of heat. This phenomenon can be explained by the fact that a high temperature during the filling phase favors saccharification to generate a sufficient amount of dextrose, and a lower temperature favors yeast growth and fermentation. The temperature increase at the end is to stimulate saccharification to prevent a halt in fermentation, since the dextrose concentration is very low near the end of a batch.

The optimal glucoamylase profile injects the glucoamylase near the end of the filling phase rather than throughout the entire period, so that the dextrose concentration will be controlled within a certain range.

The fact that the temperature slightly increases towards the end of the batch raises the question what benefits a more significant increase in the temperature can return. In order to investigate this, the optimization problem was reformulated so that both cooling and heating of the fermenter was allowed. It was found that the optimal glucoamylase profile is exactly the same as the one shown in Fig. 4, demonstrating that heating the fermenter will not change the glucoamylase injection strategy. The optimal temperature profile with both heating and cooling shows a similar pattern as that derived for just cooling. However, there are some minor differences that can be seen in Fig. 5. For example, the temperature reaches the upper bound during the filling phase. This result reinforces the interpretation of the optimal temperature profile given above, i.e., a high temperature during the filling phase favors saccharification, while a lower temperature favors fermentation, and the final increase in temperature stimulates saccharification. Allowing heating and cooling of the fermenter increases the operating expense of a facility; however, there is only a marginal benefit in the final yield of ethanol. Based upon this, the benefits provided by heating and cooling the fermenter do not justify the additional costs and only cooling the fermenter will be sufficient in practice.

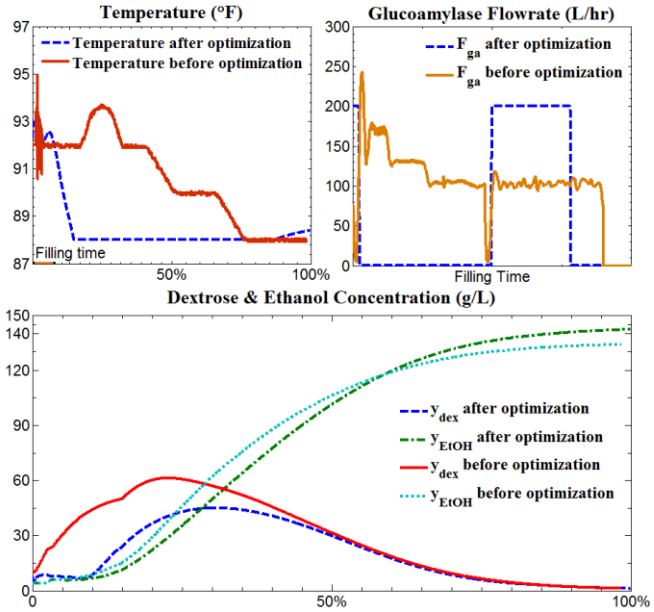

Fig. 4. Optimal input profiles and simulation result after optimization.

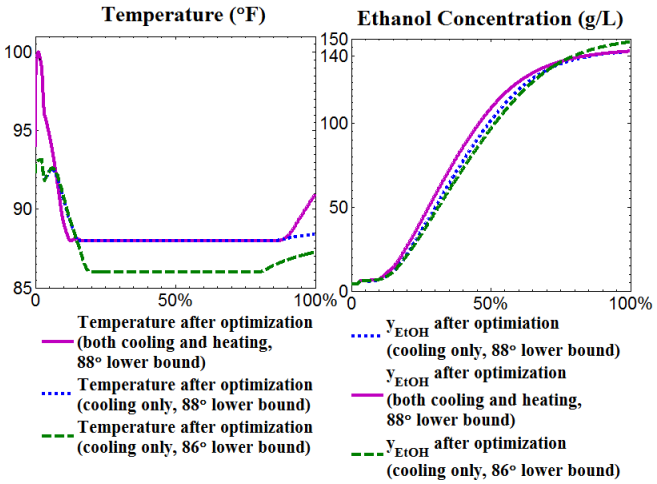

Fig. 5. Comparison of the results of the optimized profiles for a process where only cooling is allowed, the process where cooling and heating can be performed, and the original profiles.

It can be seen from the optimal temperature profile that the temperature remains at the lower bound for a majority of the batch. Due to this, it is important to investigate what effect a change in the lowest allowable temperature has on the ethanol yield. Figure 5 shows the optimal temperature profile for a lower bound of 86ºF. It can be seen that the temperature profiles retain a similar shape as before but that the profile still remains at the lower bound for extended periods of time. Similar results are found when the lower bound is further relaxed to a temperature of 84ºF. In both of these cases, the ethanol yield has improved significantly over the original one, which suggests that keeping the temperature at a reasonably

low level shortly after conclusion of the filling phase could be considered. That being said, it is important to note that the model parameters were estimated from data which came from processes that operated at a temperature at or above 88ºF, and optimization results that show that a process should be operated at a lower temperature should be taken with a grain of salt. Nevertheless, the results are suggestive and point towards some modifications that can potentially improve ethanol yield.

It can also be seen from Fig. 4 that the optimal dextrose concentration is lower than the one where no optimization was performed. This would allow to consider increasing the source of dextrose so that more ethanol would be produced under well controlled operating conditions. The simulation results show that an increased amount of maize solids in the slurry mash will increase the final ethanol yield (see Table III).

TABLE III
COMPARISON OF DIFFERENT SCENARIOS AND ETHANOL YIELDS

Temperature	Cooling/heating	Maize solid	Optimization status	Ethanol yield
88-100°F	Cooling only	327.5 g/L	Before optimization	133.0 g/L
88-100°F	Cooling only	337.5 g/L	Before optimization	137.2 g/L
88-100°F	Cooling only	327.5 g/L	After optimization	142.2 g/L
88-100°F	Cooling & heating	327.5 g/L	After optimization	142.5 g/L
86-100°F	Cooling only	327.5 g/L	After optimization	147.9 g/L

V. CONCLUSIONS

In this study, a novel SSF model is presented that incorporates an energy-balance into a model currently used in several commercial ethanol plants. This new model allows the use of a large amount of historical temperature data for parameter estimation. The estimation algorithm presented here is based on a Trust-Region approach combined with a fixed-step Runge-Kutta method for solving the model. The simulation results fit the original experimental data well for both the training and the testing data sets.

This model was subsequently used for optimizing the process. The optimal control profile (cooling water flowrate and glucoamylase flowrate) of the SSF model is found by solving a dynamic optimization problem using a simultaneous approach. The optimal temperature profile has a high temperature during the filling time and a low temperature for the rest of the process. The optimal glucoamylase profile shows that it should be injected into the fermenter near the end of the filling phase rather than at a constant rate during the entire period. The dextrose concentration after optimization is well controlled within a reasonable range, and the ethanol concentration is increased after optimization by as much as 7%. Furthermore, relaxing the lower bound of the temperature constraint proves to be the most effective way to further increase the final yield (11% increase when the lower bound is set to 86ºF). Heating and cooling the fermenter will not result in a significantly higher ethanol yield but will require more energy and additional facilities. Increasing the solids in the slurry flow will increase the final ethanol yield, but will also increase the burden on other processes such as the upstream liquification process and downstream distillation process. While the derived model used in this investigation is based upon plant data, it is nevertheless required to validate the model predictions by actually running a plant in this fashion before any definite conclusions can be drawn. That being said, this work provided several suggestions that indicate that they can result in increased ethanol yields, and the effect of these suggestions on other parts of the plants has also been discussed.

REFERENCES

[1] G. M. Walker, "125th anniversary review: fuel alcohol: current production and future challenges," *Journal of the Institute of Brewing,* vol. 117, pp. 3-22, 2011.

[2] T. W. Patzek, "A Statistical Analysis of the Theoretical Yield of Ethanol from Corn Starch," *Natural Resources Research,* vol. 15, pp. 205-212, 2006.

[3] B. de Andrés-Toro, J. M. Girón-Sierra, J. A. López-Orozco, C. Fernández-Conde, J. M. Peinado, and F. García-Ochoa, "A kinetic model for beer production under industrial operational conditions," *Mathematics and Computers in Simulation,* vol. 48, pp. 65-74, 1998.

[4] C. G. Lee, C. H. Kim, and S. K. Rhee, "A kinetic model and simulation of starch saccharification and simultaneous ethanol fermentation by amyloglucosidase and Zymomonas mobilis," *Bioprocess and Biosystems Engineering,* vol. 7, pp. 335-341, 1992.

[5] S. Ochoa, A. Yoo, J.-U. Repke, G. Wozny, and D. R. Yang, "Modeling and Parameter Identification of the Simultaneous Saccharification-Fermentation Process for Ethanol Production," *Biotechnology Progress,* vol. 23, pp. 1454-1462, 2007.

[6] A. Mulchandani and J. H. T. Luong, "Microbial inhibition kinetics revisited," *Enzyme and Microbial Technology,* vol. 11, pp. 66-73, 1989.

[7] O. Roeva, "A genetic algorithms based approach for identification of Escherichia coli fed-batch fermentation," *Bioautomation,* vol. 1, p. 30, 2004.

[8] B. de Andres-Toro, Giron-Sierra, J., Lopez-Orozco, J., Fernandez-Conde, C, "Evolutionary optimization of an industrial batch fermentation process," *Proceedings of the Europan Control Conference*, 1997.

[9] M. S. Iyer and D. C. Wunsch, II, "Dynamic re-optimization of a fed-batch fermentor using adaptive critic designs," *IEEE Transactions on Neural Networks on,* vol. 12, pp. 1433-1444, 2001.

[10] B. Srinivasan, S. Palanki, and D. Bonvin, "Dynamic optimization of batch processes: I. Characterization of the nominal solution," *Computers & Chemical Engineering,* vol. 27, pp. 1-26, 2003.

[11] S. Kameswaran and L. T. Biegler, "Simultaneous dynamic optimization strategies: Recent advances and challenges," *Computers & Chemical Engineering,* vol. 30, pp. 1560-1575, 2006.

[12] V. M. Zavala, *Computational strategies for the optimal operation of large-scale chemical processes*, PhD Thesis, Carnegie Mellon University, 2008.

[13] R. Fourer, D. Gay, and B. Kernighan, *AMPL: A Modeling Language for Mathematical Programming*, Duxbury Press, Independence, Kentucky, 2002.

[14] A. Wächter and L. T. Biegler, "On the implementation of an interior-point filter line-search algorithm for large-scale nonlinear programming," *Mathematical Programming,* vol. 106, pp. 25-57, 2006.